Transactions of the Korean Nuclear Society Autumn Meeting
Gyeongju, Korea, October 29-30, 2015

Detection of motor abnormalities by using impedance analysis

Sung Min Shin[a], Bo Hwan Choi[a], Hyun Gook Kang[a*]
[a]*Department of Nuclear and Quantum Engineering, KAIST, 291 Daehak-ro, Yuseong-gu, Daejeon 305-701, Republic of Korea*
[*]*Corresponding author: hyungook@kaist.ac.kr*

1. Introduction

In the majority of power plant safety-related systems, including nuclear power plants (NPP), motors have been widely utilized for the driving force of active components. Since safety systems are separated from the normal operating systems, during normal operation period, these motor-driven safety-critical components are at standstill. Currently, in NPPs, full-stroke tests are periodically executed to cope with random failure of the active components based on the surveillance requirements of their technical specifications [1]. This periodic testing is expected to reveal all faults in the components, however, in case of motor operated valves (MOV) in safety-related systems, 38% of total failures are discovered on actual demand for accident mitigation [2]. This high percentage indicates that the conventional periodic testing does not reveal all faults in the components, and the risk of safety-function failure should be managed with more frequent testing or with additional means for better safety. However, it is notable that frequent testing can lead to component aging as well as time offline to conduct the testing procedure in isolation.

There have been attempts to detect potential failures that are not found through full-stroke tests, usually by measurements of vibration [3-8] or motor current signature [9-15] during the operation process. All these methods are applicable only to the in-operation components. Their applicability to the standby components is very limited. Therefore, a method that can detect potential faults without operation of the component is desirable.

In this study, frequency-domain impedance analysis is utilized for the health monitoring of the motor which is at standstill. Impedance is the ratio of voltage to alternating current. Typically it uses a voltage less than 1V, which is very small in comparison with the operating voltage. In this way the impedance of a motor can be measured without actual operation. A fault detection scheme for a motor using impedance analysis is straightforward; if the impedance of the motor is changed by any potential failure, based on correlations between the impedance characteristics and various failure types, it is possible to infer the most probable failure.

Impedance analysis provides some benefits in motor health monitoring. First, the impedance of a target motor can be measured from a distance using power lines without additional devices to the motor on-site. This remote monitoring capability is especially important in the case of NPP applications because of radioactivity near nuclear reactors. Second, this method can identify various types of motor failure based on impedance change pattern. Thanks to this capability, operators can be supported in decision making of maintenance plan. Some detected motor failures might be fixed at the detected moment, but the others may have some time flexibility in maintenance

In Section 2, an equivalent circuit (EC) development for impedance analysis is explained. Based on the developed EC, the expected impedance changes for possible failure cases are investigated in Section 3. In Section 4, the possible failure cases are reproduced and the actual impedance changes are measured. Through the comparison of calculated and measured impedance changes, the validity of the motor health monitoring method using impedance analysis is examined.

2. Equivalent circuit for impedance analysis

2.1 Equivalent circuit development

In order to estimate the causes of impedance changes, an EC of a motor needs to be developed. To develop the EC, specific motor geometry that mainly affects the impedance characteristics should be converted into the circuit elements (R, L, or C), which can express an adequate circuit. Once the circuit is developed, the EC can work like a guide map between the impedance characteristics and motor geometries. For instance, let's assume that a shifting of the first resonance frequency to the left (lower frequency) and a decrease of impedance magnitude at this frequency are observed. The cause of this impedance change can be judged as an increase of a specific capacitance that corresponds to a specific motor geometry based on the EC. On the basis of the general formula of capacitance, it is possible to deduce what physical situation (source of failure) may cause the capacitance increase.

In order to analyze a wide range of impedance changes, the EC should be able to reflect impedance characteristics beyond resonance frequency. With this purpose, Mirafzal's EC model [16, 17] is adopted. By rearranging Mirafzal's model, the single-phase EC of an induction motor reflecting low to high frequency response can be expressed, as shown in Fig. 1. Basically, this model considers the capacitive characteristics between stator winding and motor frame (denoted by the subscript sf) and between the stator windings of each phase (denoted by the subscript sw).

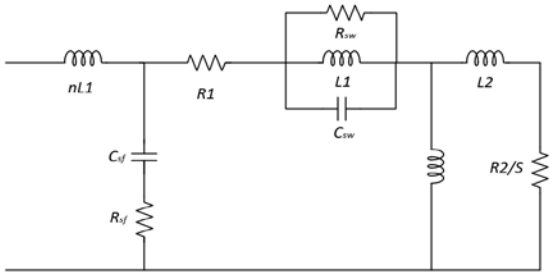

Fig. 1 Single-phase EC for high frequency response

The ECPs associated with the EC are as follow:

R_1 Stator resistance
R_2 Rotor resistance
L_1 Stator leakage inductance
L_2 Rotor leakage inductance
X_m Magnetizing inductance
S Slip
nL_1 A fraction of total stator L_1 attributed to first few turns of first slot
R_{sf} Stator copper skin effect resistance at the anti-resonance frequency
C_{sf} Effective winding-to-frame stray capacitance of first slot
R_{sw} Loss equivalent resistance at the first resonance point
C_{sw} Interturn winding capacitance

To utilize the EC for an analysis of impedance changes, it should be able to simulate the actual impedance characteristics of a target motor. For this purpose, each value of the equivalent circuit parameters (ECPs) in the EC needs to be derived properly. Among the ECPs, low-frequency response related parameters (R_1, R_2, L_1, L_2 and X_m) can generally be obtained through two tests: the no-load test which uncouples the rotor shaft from the load and the blocked-rotor test which holds the rotor from rotation [18, 19]. The high-frequency (beyond resonance) response related parameters are obtained from Mirafzal's studies [16, 17].

2.2 Validation of developed equivalent circuit

With the purpose of validating the developed EC, an induction motor is selected and the ECPs of it are obtained. The specifications of the selected motor and its derived ECPs are described in Tables 1 and 2, respectively.

Table 1 Specifications of selected induction motor

Manufacturer	CHUNIN
Model	TM-01
Phase	3-phase
Poles	4
Rated voltage [V]	380
Rated frequency [Hz]	60
Output [kW]	0.4
Winding connection	Y-connection
Rotor type	Squirrel cage rotor
NEMA class	D

Table 2 Derived values of each ECP for TM-01 induction motor

R_1[Ω]	L_1[H]	L_2[H]	L_m[H]	R_2[Ω]
2.49E1	2.50E-2	2.50E-2	5.97E-1	2.90E-1
nL_1[H]	R_{sf}[Ω]	C_{sf}[F]	C_{sw}[F]	R_{sw}[Ω]
3.10E-6	1.07E2	2.30E-10	1.80E-10	1.10E4

Over the 20 Hz-10 MHz frequency range, the impedance of the motor is measured using an impedance analyzer (KEYSIGHT, E4990A) at standstill. The EC of Fig. 1 is modeled via Matlab SIMULINK, and the impedance is calculated over the same frequency range. The measured and calculated impedance magnitude and phase angle are shown in Figures 2 and 3. As seen in these figures, the calculated impedance matches the measured impedance, except for the lumped second resonance peak. Considering though that the developed EC simulates the changing tendency of measured impedance, it is acceptable as its primary purpose is to support the theoretical background of the impedance changes for each failure case (confirmed in Section 4). Therefore, the developed EC and its ECPs are used in subsequent sections.

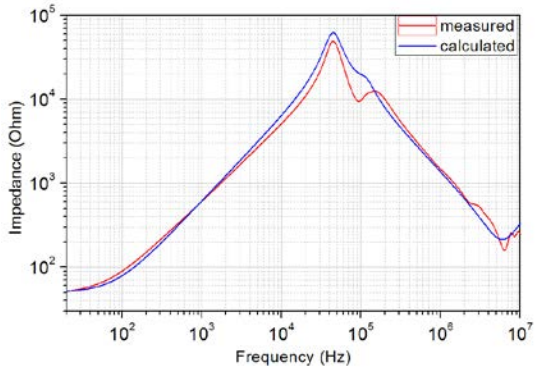

Fig. 2 Comparison of measured and calculated impedance magnitude for the experimental motor

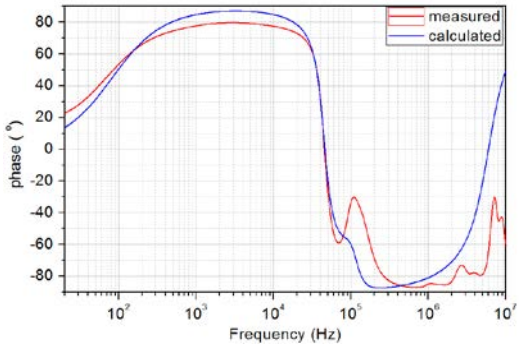

Fig. 3 Comparison of measured and calculated phase angle for experimental the motor

3. Impedance estimation for various failure cases

3.1 Motor failure cases

Prior to performing experiments, it is necessary to investigate actual motor failure cases can occur under the periodic test scheme. The U.S. Nuclear Regulatory Commission analyzed MOV failure events in U.S. NPP safety-related systems during the period from 1980 through 2000 [2]. Among the MOV failures, there are 12 motor-related failures, as shown in Table 3.

Table 3 Motor failure cases among MOV failures in US NPP safety systems

	Description
1	AFW MOVs would not fully close under high d/p conditions until the valve actuators were setup at the highest torque switch setting allowed by the tolerances.
2	RHR test return valves failed to seat tightly due to friction related problems.
3	Suppression pool cooling valves (one in each loop) failed to open. As long as the RHR pump was operating, the valves could not be opened and the thermal overloads would trip. Cause was an incorrectly sized motor.
4	Due to incorrectly sized operator the Torus cooling valves would not completely close against full differential pressure.
5	Due to the original valve operator selection criteria using less conservative factors, the outboard primary containment spray isolation valves had an inadequate torque.
6	While testing the torus suction valves, two MOVs failed when given an open signal. Both torus suction valves had shorted out due to excessive condensation in the HCI room.
7	The ECCS pump room was inadvertently flooded with water, inundating the RHR system minimum flow valve and a pump suction isolation valve. The valve operator motor windings were grounded as a result of the water intrusion.
8	Containment spray MOVs were rendered inoperable by maintenance staff error. Lubrication for the pinion gear housings was put in the motor housings.
9	Burned out motors (one LCI and one Torus cooling) due to aging.
10	Routine surveillance disclosed that the containment recirculation sump to containment spray pump isolation valves would not open. The motor for valve operators burned up.
11	Grounds were found on 2 of 4 LCI Injection valves. Probable cause was determined to be insulation breakdown.
12	None of the AFW block valves would full close against the calculated worst case d/p. The root cause of the inability of the valves is attributed to valve condition due to normal wear.

A number of these failures are not issues with the motor itself, such as switch setting (1) or friction (2) problems, and the actuator (motor) size (3, 4, and 5) problem is not applicable to the monitoring scheme, being an issue of design. Consequently, by excluding unrelated failure cases and categorizing the remaining cases, the failures can be divided largely into three categories; liquid intrusion (6, 7, and 8), burnout (9, 10), and insulation breakdown (11). For the normal wear case (12), there is no specific description. Therefore it is regarded as a complex combination of the aforementioned failure categories.

3.2 Estimation of impedance change for failure case 1: liquid intrusion Motor failure cases

Essentially, when liquid intrudes into a motor, capacitance terms (C_{sf} and C_{sw}) will be increased. Capacitance can generally be expressed as,

$$C = \frac{Q}{|\Delta V|} = \frac{\varepsilon A}{d} \quad (1)$$

where A is the overlapped area of the two plates, d is the distance between the plates, and ε is the dielectric constant of the material between the plates. When some liquid has intruded inside of the motor, it will locate between the windings and between winding and frame where air was originally located. In this situation, A or d will remain almost unchanged, but might increase significantly because the dielectric constant of liquid is much higher than that of air. In particular, the dielectric constant of water is about 80 times that of air at 1 atmosphere and room temperature. Although there may be a difference depending on the type of liquid, generally the capacitance terms (C_{sf} and C_{sw}) will be increased.

In addition to the increase of capacitance terms, the loss equivalent resistance (R_{sw}) at the first resonance frequency will also be reduced, as the electrical resistance of liquid is generally smaller than that of air. Although the significance of this effect is difficult to calculate numerically as a result of the effects of winding complexity and the insulation jacket, in effect R_{sw} will be reduced.

With these estimates, the values of C_{sw}, C_{sf}, and R_{sw} are modified properly ($C_{sw} = 3.8\text{E}-10$, $C_{sf} = 4.6\text{E}-10$, $R_{sw} = 5.5\text{E}3$) from the values in Table 2 and applied to the developed EC. Then the impedance magnitude and phase angle are recalculated and shown in Figures 4 and 5.

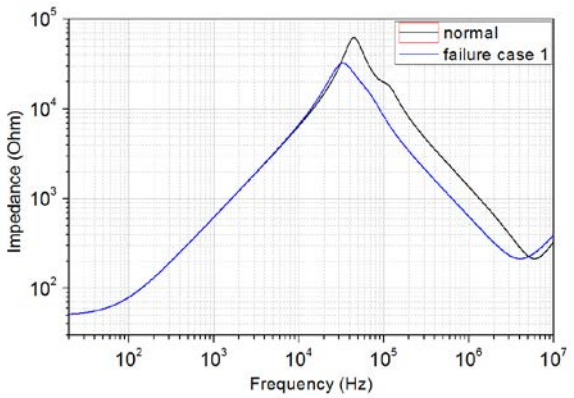

Fig. 4 Estimation of the impedance magnitude change for the liquid intrusion case

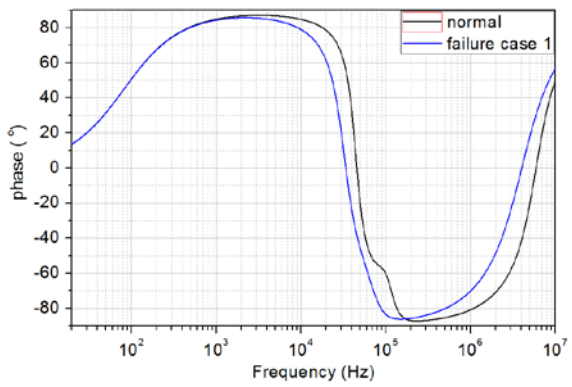

Fig. 5 Estimation of the phase angle change for the liquid intrusion case

Some noticeable changes are observed in the first resonance region while the low frequency response is nearly the same. The resonance frequency shifts to the left (lower frequency region), and the impedance magnitude at this frequency decreases in comparison with the normal case. The frequency at the resonance region (f_r) can simply be expressed as Equation 2; on the basis of this equation, the increased capacitance leads to a decrease (shift to the lower frequency) of the resonance frequency. The reduced R_{sw} would serve to decrease the impedance magnitude at this resonance frequency.

$$f_r = \frac{1}{2\pi\sqrt{LC}} \quad (2)$$

3.3 Estimation of impedance change for failure case 2: burnout

Burnout typically occurs in the stator winding, which is a bundle of thin wires. When the motor is running, the temperature of the stator winding rises drastically because of substantial heat loss coupled with poor dissipation. As the temperature rises, the insulation can be easily destroyed. After burnout, a short-circuit between windings is usually found; more specifically, this refers to a connection of each winding turn of a single phase or different phase lines in addition to the neutral point.

When the stator windings are burned out, changes in many ECPs (L_m, L_1, L_2, R_1, R_{sw}, and C_{sw}) in the EC can be expected. When there is a short-circuit between windings, the number of turns will reduce and it leads to a decrease of L_m because the inductance is basically proportional to the square of the number of winding turns. The decreased L_m is directly related to the leakage inductances of stator (L_1) and rotor (L_2). A short-circuit also shortens the path of low-frequency current flow which leads to a reduction of R_1. C_{sw} and corresponding R_{sw} are also reduced by reducing the area term of expression of capacitance.

With these estimates, the values of L_m, L_1, L_2, R_1, R_{sw}, and C_{sw} are modified properly ($L_m = 2.99\text{E}-1$, $L_1 = 1.25E-2$, $L_2 = 1.25E-2$, $R_1 = 1.25E1$, $R_{sw} = 5.5\text{E}3$, $C_{sw} = 9\text{E}-11$) from the original values. After applying the modified values to the EC, the impedance magnitude and phase angle are recalculated and shown in Figures 6 and 7.

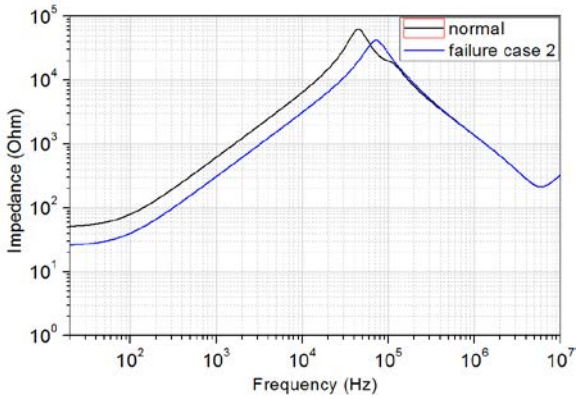

Fig. 6 Estimation of the impedance magnitude change for the burnout case

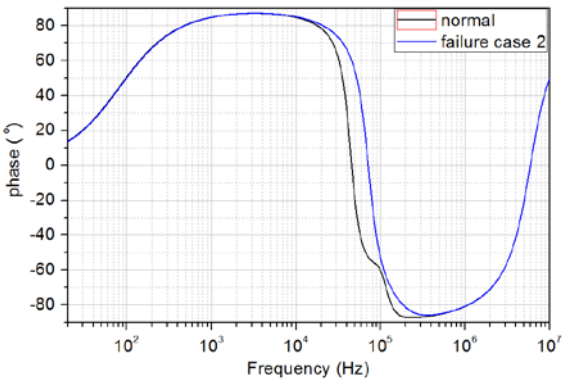

Fig. 7 Estimation of the phase angle change for the burnout case

The apparent changes in impedance characteristics can be clearly distinguished from the case of liquid intrusion. The impedance magnitude has been reduced in the low frequency region, which is associated with the reduction of R_1 and inductances. The shifting of the resonance frequency to the right side (higher frequency region) is also observed. The reasons for this shifting are a reduction in C_{sw} and inductances, confirmed through Equation 2. Lastly, a decrease in impedance magnitude at the resonance frequency is observed. The reduced R_{sw} can be inferred as the cause for this change.

3.4 Estimation of impedance change for failure case 3: insulation breakdown

Failure case 11 in Table 3 does not provide a detailed description about the failure despite the ambiguity of an insulation breakdown. In order to analyze this failure, general cases are investigated. Insulation breakdown can be roughly divided into two cases: breakdown occurring inside of the motor housing, and outside of the motor

housing (lead lines). Inside insulation breakdown may be caused by a mechanical impact, corrosion due to foreign material intrusion, or excessive operation. The only cause of a mechanical impact to the inside of the motor housing is the rotation of the rotor. Such an impact can surely be detected through a pretest, so there will be no additional impact to the inside of the motor as long as it is protected by the housing. Corrosion of the insulator is to be preceded by the intrusion of an external liquid, which can be identified by the detection method for failure case 1. Moreover, insulation breakdown caused by excessive operation can be covered by the detection method for failure case 2. Therefore, in this section, only the insulation breakdown of lead wires (short-circuit and disconnection) is considered.

If a short-circuit occurs between lead lines, there will be no resonance region in the impedance magnitude since all the capacitive characteristics disappear. The impedance will simply increase alongside the frequency because of inductive reactance. The impedance magnitude of the low frequency region will be very small as only the resistance of the lead line will exist instead of stator winding resistance.

In the case of disconnection of lead lines, except for instability of impedance, it is difficult to estimate the specific characteristics.

4. Reproduction of failure cases and confirmation of impedance changes

4.1 Confirmation of impedance change for failure case 1: liquid intrusion

Failure case 1 is covered by the water vapor condensation test as water or lubrication intrusion can be considered as more serious condition of condensation. IEEE has published a standard for test procedures for the evaluation of AC electric machinery [21], and in this standard there are descriptions of moisture exposure tests. As recommended in this standard, in order to cause condensation on the motor winding, an enclosing hood is applied and the floor under the hood is covered with a shallow layer of water heated ten degrees above the motor body temperature. After 48 hours, uniform and visible condensation on the winding can be verified (Fig. 8).

Fig. 8 Figure of normal windings (left) and windings with condensation (right)

The impedance magnitude and phase angle of a motor with condensation on the stator windings are measured through the impedance analyzer and shown in Figures 9 and 10. The tendencies of changes in impedance magnitude and phase angle are exactly the same as the calculated ones based on the EC (Figs. 4 and 5). This comparison validates the developed EC and the estimates about impedance changes for failure case 1. As a result of the experiment, it can be said that liquid intrusion to the motor might be detected through impedance analysis based on the identified impedance change tendency.

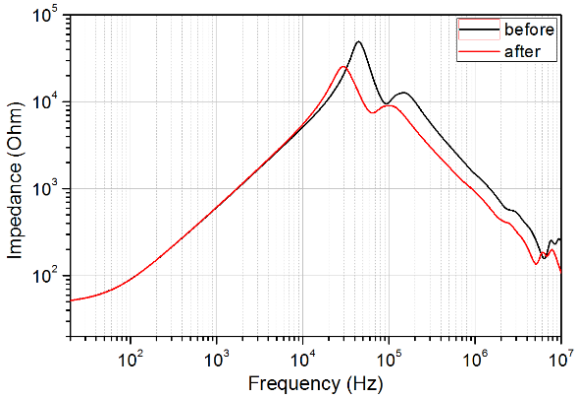

Fig. 9 Measured impedance magnitude before and after water vapor condensation

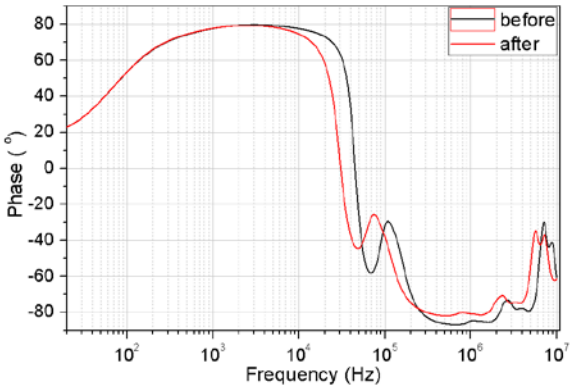

Fig. 10 Measured phase angle before and after water vapor condensation

4.2 Confirmation of impedance change for failure case 2: burnout

Motor burnout may occur when rated voltage is continuously applied to a motor that cannot rotate. This situation is mainly due to incorrect settings of the switch elements such as torque or limit switch in a MOV. To reproduce this failure, rated voltage is applied after blocking the rotor. In order to exclude measurement error due to the high temperature and hysteresis, the impedance characteristics along the frequency are measured 24 hours after the experiment at 25°C. Figures 12 and 13 show the impedance magnitude and phase angle of the motor before and after the experiment, respectively. The tendency of impedance change for this failure case is also almost the same as the calculated one based on the EC in Section 3.3, demonstrating a shifting

of resonance frequency to the high-frequency region, and a reduction of impedance magnitude at this resonance frequency as well as at the very low-frequency region. Based on the identified tendencies, motor burnout might be detected through impedance analysis.

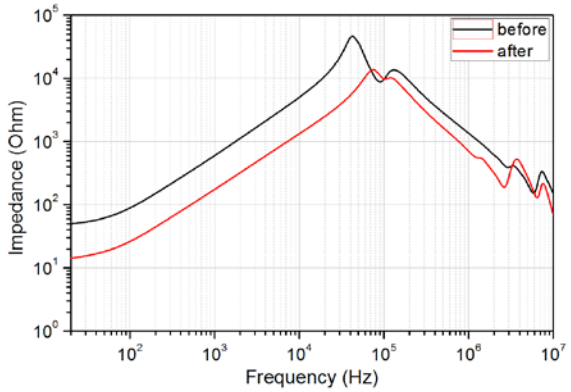

Fig. 11 Measured impedance magnitude before and after burnout

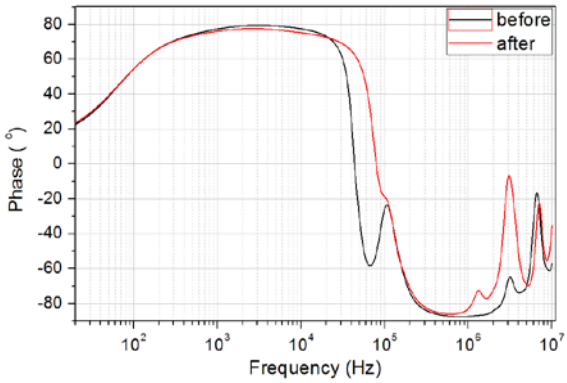

Fig. 12 Measured phase angle before and after burnout

After the impedance measurements, the inner side of the motor is observed by disassembling the housing. As shown in Fig. 13, the actual burnout is confirmed on a section of the stator winding.

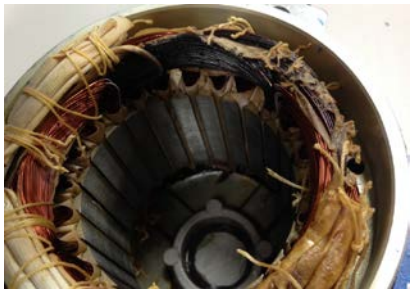

Fig. 13 Windings of a motor after burnout

4.3 Confirmation of impedance change for failure case 3: insulation breakdown

As investigated in Section 3.4, short-circuits and the disconnection of lead wires are considered for this failure case. First, the short-circuit is emulated by biting two out of the three lead wires together, and the impedance magnitude and phase angle are measured (Fig. 14). The overall shape of the impedance magnitude and phase angle along the frequency are changed significantly from the normal case. As expected, there is no resonance region, and the impedance magnitude simply increases along the frequency. Based on the change in phase angle, the main cause of impedance increase can be verified as inductive reactance. When the impedance exhibits this identified tendency, it can be inferred that a short-circuit between lead wires has occurred.

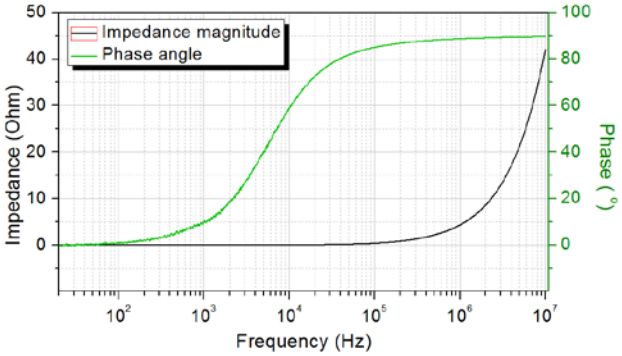

Fig. 14 Measured impedance magnitude and phase angle after short-circuit

Next, the disconnection case is emulated by opening one phase line from the terminal of the impedance analyzer. Impedance magnitude and phase angle are measured and shown in Fig. 15. In the low-frequency region, the phase angle goes to the extreme maximum and minimum continuously along the frequency. This phenomenon represents a disconnection of lead wires because it cannot physically occur in a normal closed circuit. Note that the convergences of impedance magnitude to zero and phase angle to -90^{o} are merely capacitive characteristics between two terminals of the impedance analyzer.

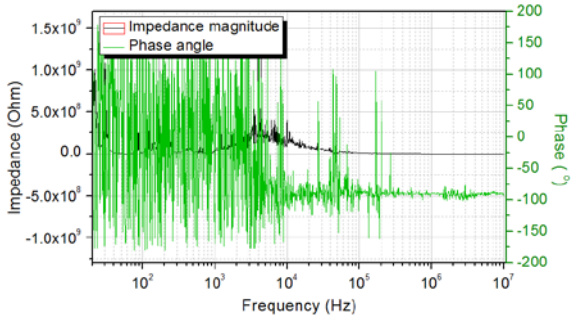

Fig. 15 Impedance magnitude and phase angle after lead wire disconnection

5. Conclusions

Although monitoring all elements comprising active components is ideal, at minimum, specific crucial elements should be continuously monitored to prevent complete failure. In this study, an impedance analysis for

motor health monitoring at standstill was suggested. With this purpose, the correlations between impedance characteristics and various failure types were estimated based on the developed EC, and experimentally validated. Changes in impedance characteristics for each failure case were clearly observed, and the changing tendencies were also distinguishable for each failure case. On the basis of these results, it was confirmed that the impedance analysis can be used for motor failure detection.

The suggested method can obtain information about motor condition without actual operation of the active component, thereby addressing problems such as aging effects and time offline to conduct the testing procedure in isolation. The method is suitable for the component located in inaccessible area because the impedance can be measured from a distance by using power lines without additional device to the target motor. In addition, this method can detect different types of failure as long as the correlations between the impedance characteristics and the failures are identified.

This method is expected to be applied to all the components that are operated by motors, such as motor-operated valves and motor-driven pumps. This monitoring method can also be applied to the previously developed quantitative analysis for the availability of a standby component with the periodic test scheme [22].

REFERENCES

[1] M. Čepin and B. Mavko, "Probabilistic safety assessment improves surveillance requirements in technical specifications," Reliab. Eng. Syst. Saf., vol. 56, no. 1, pp. 69–77, 1997.
[2] NRC, "Common-Cause Failure Event Insights Motor-Operated Valves," vol. 2, 2003.
[3] J. R. Cameron, W. T. Thomson, and a. B. Dow, "Vibration and current monitoring for detecting airgap eccentricity in large induction motors," IEE Proc. B Electr. Power Appl., vol. 133, no. 3, p. 155, 1986.
[4] J. R. Stack, T. G. Habetler, and R. G. Harley, "Effects of machine speed on the development and detection of rolling element bearing faults," IEEE Power Electron. Lett., vol. 1, no. 1, pp. 19–21, 2003.
[5] S. a. McInerny and Y. Dai, "Basic vibration signal processing for bearing fault detection," IEEE Trans. Educ., vol. 46, no. 1, pp. 149–156, 2003.
[6] J. Zarei, M. A. Tajeddini, and H. R. Karimi, "Vibration analysis for bearing fault detection and classification using an intelligent filter," Mechatronics, vol. 24, no. 2, pp. 151–157, 2014.
[7] V. Climente-Alarcon, J. a. Antonino-Daviu, F. Vedreño-Santos, and R. Puche-Panadero, "Vibration transient detection of broken rotor bars by PSH sidebands," IEEE Trans. Ind. Appl., vol. 49, no. 6, pp. 2576–2582, 2013.
[8] T. Li and Z. Zhang, "Vibration data processing based on petri network in wireless sensor networks," J. Networks, vol. 7, no. 2, pp. 400–407, 2012.
[9] R. R. Schoen, B. K. Lin, S. Member, T. G. Habetler, S. Member, J. H. Schlag, and S. Farag, "An Unsupervised, On-line System for Induction Motor Fault Detection Using Stator Current Monitoring," IEEE Trans. Ind. Appl., vol. 31, no. 6, pp. 1280–1286, 1995.
[10] B. Yazict, G. B. Kliman, W. J. Premerlani, R. a Koegl, G. B. Robinson, and A. Abdel-malek, "An Adaptive , On-line , Statistical Method for Bearing Fault Detection Using Stator Current," 1997.
[11] G. H. Müller and C. F. Landy, "A novel method to detect broken rotor bars in squirrel cage induction motors when interbar currents are present," IEEE Trans. Energy Convers., vol. 18, no. 1, pp. 71–79, 2003.
[12] S. Kang, S. Park, D. Lee, and Y. Kim, "Motor control center based technology study for safety-related motor operated valve," Nucl. Eng. Technol., vol. 38, no. 2, pp. 155–162, 2006.
[13] E. C. C. Lau and H. W. Ngan, "Detection of motor bearing outer raceway defect by wavelet packet transformed motor current signature analysis," IEEE Trans. Instrum. Meas., vol. 59, no. 10, pp. 2683–2690, 2010.
[14] G. M. Joksimovic, J. Riger, T. M. Wolbank, N. Peric, and M. Vasak, "Stator-current spectrum signature of healthy cage rotor induction machines," IEEE Trans. Ind. Electron., vol. 60, no. 9, pp. 4025–4033, 2013.
[15] Y. Da, X. Shi, and M. Krishnamurthy, "A new approach to fault diagnostics for permanent magnet synchronous machines using electromagnetic signature analysis," IEEE Trans. Power Electron., vol. 28,
[16] B. Mirafzal and G. Skibinski, "Universal induction motor model with low-to-high frequency-response characteristics," IEEE Trans. Ind. Appl., vol. 43, no. 5, pp. 1233–1246, 2007.
[17] B. Mirafzal, S. Member, G. L. Skibinski, and R. M. Tallam, "Determination of parameters in the universal induction motor model," IEEE Trans. Ind. Appl., vol. 45, no. 1, pp. 142–151, 2009.
[18] A. E. Fitzgerald, J. Charles Kingsley, and S. D. Umans, Electric machinery. 2003.
[19] Franklin H. Grooms, IEEE Standard Test Procedure for Polyphase Induction Motors and Generators, IEEE Std 112-2004. 2004.
[20] M. Uematsu and E. U. Frank, "Static Dielectric Constant of Water and Steam," J. Phys. Chem. Ref. Data, vol. 9, no. 4, p. 1291, 1980.
[21] Robert D. Briskman, IEEE Standard Test Procedure for Evaluation of Systems of Insulating Materials for Random-Wound AC Electric Machinery, IEEE Std 117-1974. 1992.
[22] S. M. Shin, I. S. Jeon, and H. G. Kang, "Surveillance test and monitoring strategy for the availability improvement of standby equipment using age-dependent model," Reliab. Eng. Syst. Saf., vol. 135, pp. 100–106, 2015.